Modular assembly of superstructures from polyphenol-functionalized building blocks

Junling Guo[1,2], Blaise L. Tardy[1,2], Andrew J. Christofferson[3], Yunlu Dai[1,2], Joseph J. Richardson[1,4], Wei Zhu[2,5], Ming Hu[2,6], Yi Ju[1,2], Jiwei Cui[1,2], Raymond R. Dagastine[2], Irene Yarovsky[3] and Frank Caruso[1,2,*]

[1]ARC Centre of Excellence in Convergent Bio-Nano Science and Technology, The University of Melbourne, Parkville, Victoria 3010, Australia.

[2]Department of Chemical and Biomolecular Engineering, The University of Melbourne, Parkville, Victoria 3010, Australia.

[3]School of Engineering, RMIT University, GPO Box 2476, Victoria 3001, Australia.

[4]Present address: CSIRO Manufacturing Flagship, CSIRO, Clayton South, Victoria 3169, Australia.

[5]Present address: Advanced Materials Laboratory, Sandia National Laboratories, Albuquerque, New Mexico 87185, United States.

[6]Present address: Department of Physics, Center for Functional Nanomaterials and Devices, East China Normal University, Shanghai 200241, China.

*E-mail: fcaruso@unimelb.edu.au

The organized assembly of particles into superstructures is typically governed by specific molecular interactions or external directing factors associated with the particle building blocks, both of which are particle-dependent. These superstructures are of interest to a variety of fields because of their distinct mechanical, electronic, magnetic and optical properties. Here, we establish a facile route to a diverse range of superstructures based on the polyphenol surface-functionalization of micro- and nanoparticles, nanowires, nanosheets, nanocubes and even cells. This strategy can be used to access a large number of modularly-assembled superstructures, including core-satellite, hollow, and hierarchically-organized supraparticles. Colloidal-probe atomic force microscopy and molecular dynamics simulations provide detailed insights into the role of surface functionalization and how this facilitates superstructure construction. Our work provides a platform for the rapid generation of superstructured assemblies across a wide range of length scales, from nanometres to centimetres.

The assembly of complex superstructures from simple building blocks is of widespread interest for engineering materials with enhanced and synergistic properties[1-4]. Such materials have potential application in drug delivery[5], photonics[6], chemical sensing[7], energy storage[8], gas adsorption[9], and catalysis[10]. Superstructuring is also of fundamental importance for improving our understanding of self-assembly processes in biological systems, which occur on molecular-to-macroscopic length scales[11,12]. From a fundamental perspective, current particle-based assembly methods are particle-dependent owing to the diverse types and properties of particles available (e.g., composition, size, shape, and surface chemistry)[13-16]. These challenges are often overcome on a case-by-case basis to create particle-based superstructures using various methods including interfacial assembly[17], layer-by-layer (LbL) assembly[18], terminal supraparticle assembly[19], ligand-driven assembly[20,21], evaporation assembly[22], and DNA-based assembly[23-25]. These methods require highly specific assembly mechanisms to control microscale interactions to endow the particles with selective molecular interactions for driving assembly (e.g., DNA hybridization[25,26] and antibody-antigen specificity[27]) and/or external physical factors (e.g., interfacial assembly, confined geometries, and magnetic properties)[14]. There is a need to develop methods to control microscale particle interactions that can overcome the constraint of particle-specific assembly, thus providing greater versatility in the resulting assemblies of superstructures by both relaxing the requirements for and broadening the choice of building components.

Here we explore the use of polyphenol-based surface functionalization to develop a facile and straightforward strategy that transforms diverse materials into modular superstructure components that behave akin to what we encounter with macroscopic building blocks such as bricks and mortar or LEGO bricks. This method comprises two steps: particle surface functionalization with polyphenol moieties, which has been shown to be independent of the substrate/particle surface chemistry largely because of the multidentate properties of

polyphenols (**Fig. 1a–c**, **Supplementary Fig. S1**)[28,29], followed by particle assembly directed by interfacial molecular interactions and inter-particle locking of the functionalized particles using metal ions (**Fig. 1d–h**). The simplicity and modularity of this approach enable the transformation of 15 representative materials, with different sizes, shapes, compositions, and functionalities (i.e., polymeric particles, metal oxide particles and wires, noble metal nanoparticles, upconversion nanoparticles, coordination polymer nanowires, nanosheets, nanocubes, cells) into building blocks for the construction of complex three-dimensional (3D) superstructures, including core–satellite, hollow, hierarchically organized supraparticles, and macroscopic hybrid materials. An additional benefit of our system is that the superstructures are linked via coordinating with different metal ions, thus affording superstructures with chemical diversity and structural tailorability (**Fig. 1h**). Owing to their natural origin and relative abundance[30], polyphenols are inexpensive, green, and easily accessible scaffolds for superstructure construction, especially when compared with currently used DNA aptamers, clonal antibodies, or synthetic polymers[20,31]. Molecular dynamics (MD) simulations and colloidal-probe atomic force microscopy (AFM) provide insights into the mechanism of polyphenol-based particle functionalization and understanding the roles of polyphenols on particle assembly and the inter-particle locking process.

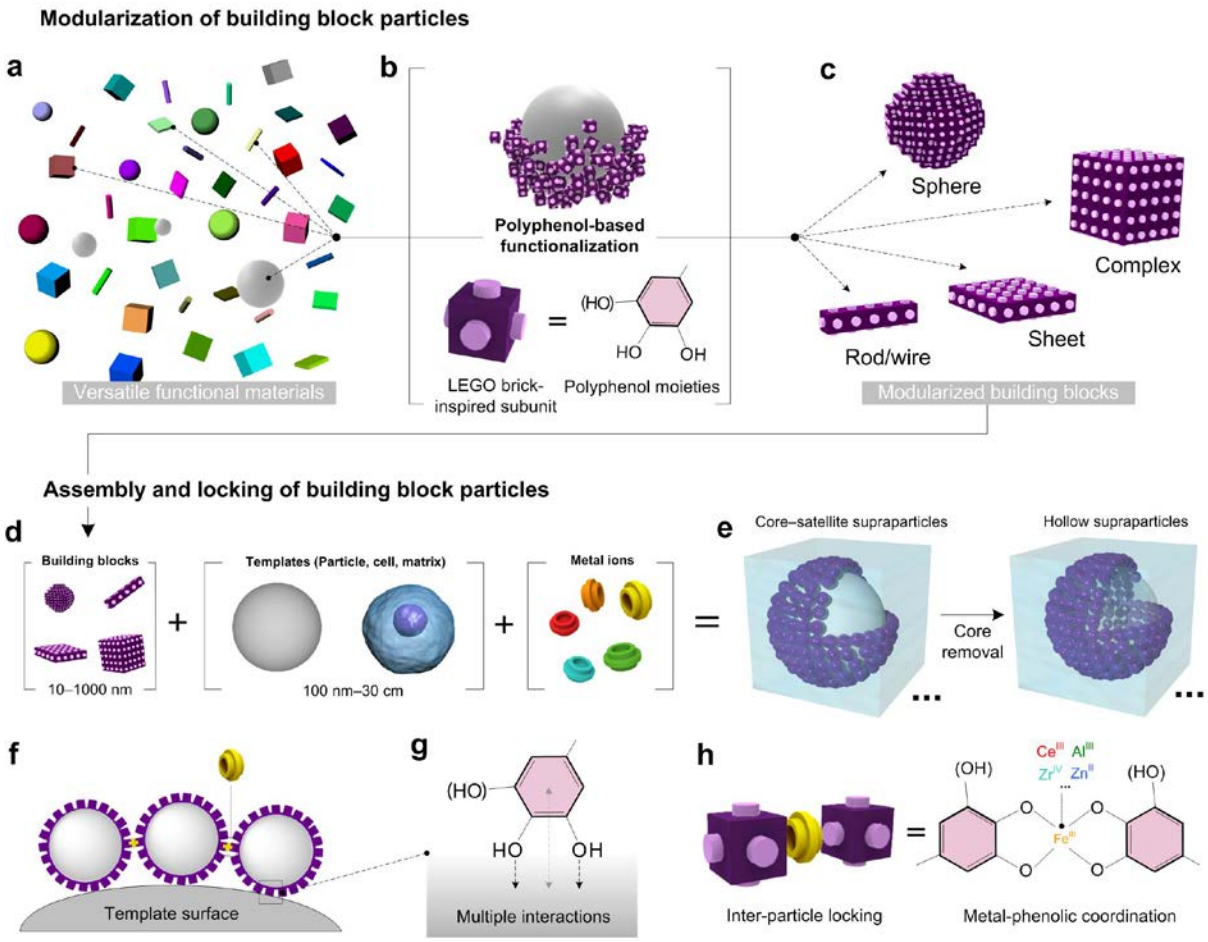

Figure 1. Modularization, assembly, and inter-particle locking of building blocks analogous to LEGO bricks. a, Schematic of versatile materials with different shapes, structures, compositions, and functionalities. **b**,**c**, LEGO brick-inspired modularization of building blocks through polyphenol-based particle functionalization. **d**,**e**, Modular assembly of core–satellite and hollow supraparticles with a selection of versatile modularized building blocks, templates, and metal ions. **f**,**g**, Assembly of building blocks on core particles using interfacial molecular interactions between polyphenol moieties and the substrate. **h**, Schematic and molecular structure of LEGO brick-inspired linkage between polyphenol-functionalized particles.

Modular assembly of spherical building blocks

The primary advantage of the current process is that it establishes a wide range of micro- and nanomaterials as robust and modular components for constructing superstructures, simply through particle surface functionalization. The high dihydroxyphenyl (catechol, C) or trihydroxyphenyl (galloyl, G) content of natural polyphenols is of interest in the context of particle surface functionalization (**Supplementary Fig. S1**), as polyphenols are known to

strongly bind to diverse surfaces (e.g., metal oxides, noble metals, and polymeric substrates) through covalent and noncovalent interactions[32]. After the polyphenol-based functionalization of particles, the functional C/G groups of polyphenol create the building blocks with similar surface chemistries; these G/C groups are analogous to the unified studs in LEGO bricks (**Fig. 1b,c**). Moreover, these C/G studs can interact with a secondary substrate, providing the particle assembly driving force on coordination with metal ions that are involved in inter-particle connections (**Fig. 1f–h**). In a typical experiment for the modular assembly of superstructures, building block particles were first synthesized using established methods (**Supplementary Section S2**). Then, their surfaces were functionalized with C/G groups via either (1) the use of a coordination-based metal-phenolic network (i.e., complexation between Fe^{3+} ions and tannic acid (TA) to form an iron-phenolic network, FePN)[28] or (2) oxidation reactions of polyphenols (i.e., from dopamine to polydopamine, PDA)[29] (**Fig. 1b, Supplementary Fig. S2**). Transmission electron microscopy (TEM) revealed the presence of a nanoshell coating on the building blocks after particle functionalization (**Supplementary Fig. S3**); the coating did not affect their monodispersity, as monitored by two-dimensional (2D) light-scattering mapping (**Supplementary Fig. S4**). The FePN- or PDA-functionalized particles were then assembled into superstructures by mixing them with larger templates (i.e., bare polystyrene particles (PS), cells, macroscopic matrix) in aqueous solution. During assembly of the building blocks onto the template, the addition of metal ions instigates metal-phenol complexation between the building block particles, locking them in place. The interconnecting coordination was confirmed by the changes of metal concentrations (**Supplementary Fig. S5**)[28]. Differential interference contrast (DIC) microscopy showed the monodisperse core (10 μm PS)–satellite (1 μm SiO_2) supraparticles denoted as $^{10}PS@^{1}SiO_2$ (**Fig. 2a**). Additionally, super-resolution structured illumination microscopy revealed the 3D superstructure of $^{10}PS@^{0.5}MF$ supraparticles constructed from fluorescent melamine resin

(MF) particles (**Fig. 2b,c**); it is apparent that the particles are efficiently packed around the core template (**Fig. 2d**).

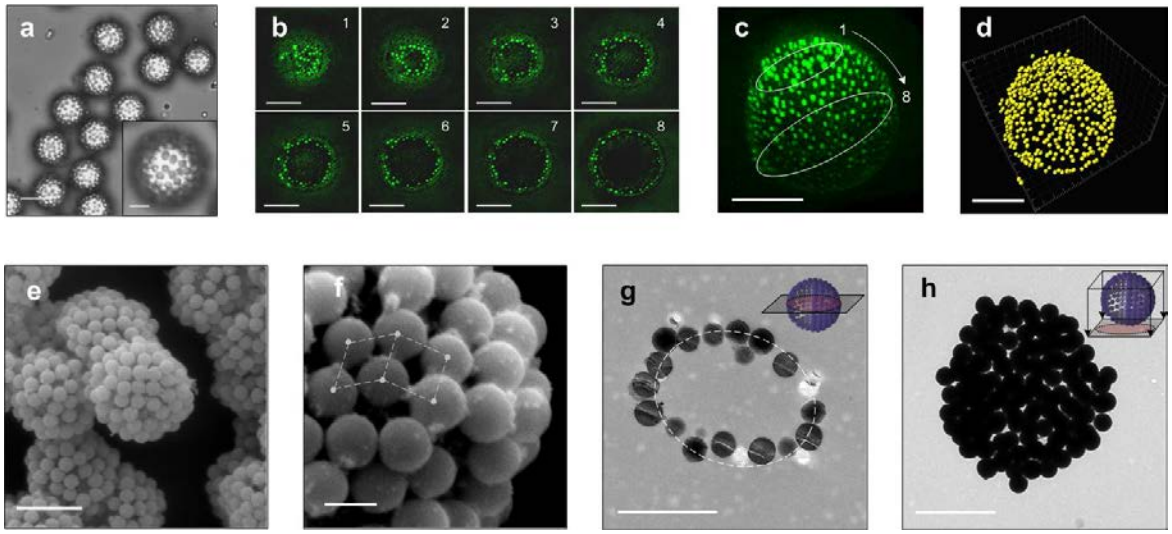

Figure 2. Modular assembly of SiO_2, fluorescent melamine resin (MF) particles, and polystyrene (PS) particles into spherical 3D superstructures. a, Differential interference contrast (DIC) images of core–satellite $^{10}PS@^{1}SiO_2$ supraparticles (scale bars are 10 μm and 2 μm in the inset image). **b–d**, Sliced, 3D structured illumination microscopy (SIM) images, and reconstructed model of core–satellite $^{10}PS@^{0.5}MF$ supraparticles (scale bars are 5 μm). **e**,**f**, SEM images of hollow $^{0.3}SiO_2$ supraparticles prepared through critical point drying (CPD) technique (scale bars are 2 μm in **e** and 500 nm in **f**). **g**,**h**, TEM images of hollow $^{0.3}SiO_2$ supraparticles prepared as ultra-thin sliced (**g**) and air-dried (**h**) specimens (scale bars are 2 μm).

After removal of the core template (e.g., removing PS particles by washing with tetrahydrofuran), the arrangement of the building particles could be stabilized to maintain a spherical superstructural architecture (**Fig. 1e–h**). Critical point drying (CPD)-assisted scanning electron microscopy (SEM) showed the 3D spherical structure of $^{0.3}SiO_2$ supraparticles and densely packed building blocks (**Fig. 2f**). The hollow structure was observed by TEM imaging of ultra-thin cross-sectional specimens (**Fig. 2g**), whereas the 2D projection of the overall superstructure was visible using TEM imaging on air-dried samples (**Fig. 2h**). The entire modular assembly could be achieved within approximately 10–15 min for FePN-coated and ~2 h for PDA-coated building blocks (**Supplementary Fig. S6**), thus

highlighting the efficiency of this process and the versatility of surface chemistry in this method. In this study, the coordination-based polyphenol network was selected as the main method for particle functionalization, owing to its exceptionally rapid processing, disassembly properties, and negligible cytotoxicity[28].

Mechanism of modular assembly

As shown in **Fig. 3a–c**, the formation of supraparticles consists of two steps: assembly of C/G-functionalized building blocks on a larger template and metal coordination-based inter-particle locking. Colloidal-probe AFM was first used to examine in detail the forces acting during the assembly process (**Fig. 3d,e**). The colloidal probe was first coated with FePN, as used for the surface functionalization of the building blocks. An approach–retraction loop was used to probe the interactions when the C/G-functionalized building block particles approached the template. As shown in **Fig. 3d**, as the FePN-coated probe approached the bare PS particles (10 μm; zeta potential (ζ) = −2 mV), a weak repulsion, followed by a short-range attraction were observed. These results indicate that the attractive forces between the C/G-functionalized particles and template substrate are the main factors governing particle assembly. The effect of template surface charge was then examined using bare PS particles with a more negative surface potential (50 μm; ζ = −30 ± 3 mV). **Fig. 3e** demonstrates that these particles ($PS^{\delta-}$) had consistently a larger repulsion range owing to an electrical double layer force. Therefore, the negatively charged FePN (ζ = −18 ± 4 mV) prevented the C/G-functionalized surface from experiencing ubiquitous interfacial interactions, consequently preventing particle assembly from occurring. Adhesive forces were observed in the retraction or unloading portion of the force loop. These forces have a longer range and higher maxima in the case of the 10-μm particles (average energy dissipated in the form of work of adhesion, $E_d = 2.24 \times 10^{-1}$ fJ) when compared with those in the case of the 50-μm particles ($E_d = 5.99 \times$

10^{-2} fJ). The high dissipation energies also confirmed that the superstructuring is a process driven by attractive interactions. This also supports the high versatility and stability of supraparticles and may explain why the particles are not assembled with a perfect packing **(Supplementary Fig. S7)**[33].

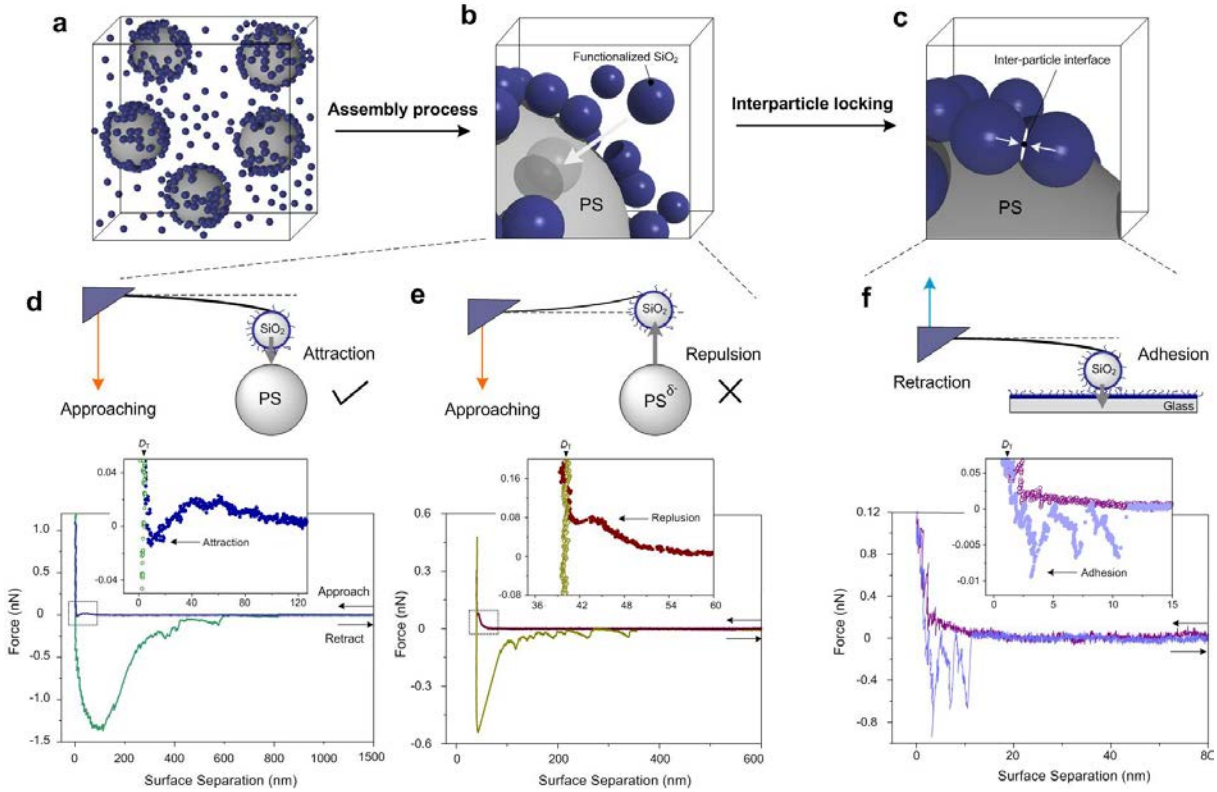

Figure 3. Colloidal-probe AFM studies of modular assembly. a–c, Schematic of disperse building block particles and large core templates (**a**), assembly of building block particles on the surface of core templates (**b**), and inter-particle locking of assembled building block particles on core templates (**c**). **d**,**e** Schematic and representative force–distance curves of FePN-coated SiO_2-attached probes approaching bare PS particles with neutral (**d**) and negative (**e**) surface charges. **f**, Schematic and representative force–distance curves of FePN-coated SiO_2-attached probe approaching an FePN-coated planar glass substrate.

Some insights into the inter-particle locking between two FePN surfaces were obtained by bringing into contact an FePN-coated colloidal probe with an FePN-coated glass substrate. As shown in **Fig. 3f** and **Supplementary Fig. S8**, a consistent repulsive potential was seen during the approach. In contrast, during retraction, adhesive forces, comprising successive

tooth-like adhesive jumps, reminiscent of breaking sacrificial bonds from modular polymer structures or inter-digitation of the two coatings, were observed[34]. These results suggest that close contact of the building block particles is essential for inter-particle locking to occur upon addition of metal ions. It is likely that the repulsive potential between FePN-coated particles is less than the attraction of these particles with larger PS particles. Therefore, collision events between the building blocks and core templates likely lead to the assembly process regardless of the close proximity of other adsorbed FePN-coated particles. This has similarities with the recent report by Liebler and co-workers[35], where bare particles can be used as an adhesive to bridge different organic materials, such as polymers, hydrogels and even tissue; in our study the polyphenol complexes are used as the linker or "adhesive" as opposed to bare particles.

To further understand the interfacial molecular interactions occurring during particle functionalization and assembly, and in particular the key role of the coordination of Fe during these processes, MD simulations were performed on TA_3 clusters and Fe^{III}-TA_3 complexes (FePN) interacting with PS surfaces (**Supplementary Section S10** and **Notes and Discussion**). Regardless of the presence of Fe, the adsorption of TA on the PS surface occurred in a stepwise fashion typical of hydrophobic surfaces[36]. The initial step in adsorption is the anchoring of the C/G groups to the PS–water interface at an angle larger than 45° with respect to the plane of the PS surface (**Supplementary Fig. S9a**). This process is followed by π-π stacking between the C/G aromatic groups and PS benzene rings. Lockdown occurs as the number of (C/G)-PS aromatic contacts increase and the contact area between the PS surface and TA_3 or Fe^{III}-TA is desolvated (**Supplementary Fig. S9a–c**). Once lockdown occurs, there is no lateral movement of TA_3 or Fe^{III}-TA_3 across the PS surface. These results agree with the literature, which shows that polymer chains can reorganize and dissipate energy onto the surface of nanoparticles to provide a strong net connection at particle–polymer interfaces[35,37].

Another significant finding was that in ~60% of the sampled adsorption configurations, one TA of Fe^{III}-TA_3 remained unadsorbed on the PS surface and extended up to 4.5 nm away from the PS interface (**Supplementary Fig. S9d** and **Notes and Discussion**). This extended TA domain could provide an anchoring point for secondary interactions with templates or inter-particle bridging through complexation with Fe^{3+} ions in solution. However, this extension was not observed in adsorbed TA_3 clusters, as TA tend to be found in greater concentrations at the PS interface without a similar degree of outwards extension. Therefore, the coordination of Fe is essential for both the particle assembly and locking process to occur. Note that in this work, only the interactions between Fe^{III}-TA_3 complexes (FePN) and a PS-based surface were examined to demonstrate the mechanism of those processes. However, electrostatic and van der Waals forces, hydrogen bonding and, possibly, charge-transfer contribute to interactions between C/G groups and other surfaces of the building blocks and templates. Therefore, fine control of these various interactions could provide a highly versatile platform for the future design of structures and functions.

Extension of modular assembly to complex building blocks

To examine the versatility of our modular assembly strategy, diverse building block materials ranging from inorganic to organic and from spherical to complex geometries, were selected to construct hollow supraparticles. As shown in **Fig. 4a–c**, SiO_2 microparticles, mesoporous SiO_2 nanoparticles, and upconversion nanoparticles ($NaYF_4$:Yb/Er) were used for the assembly of superstructures from spherical building blocks. Hollow supraparticles could be prepared from spherical building blocks ranging from ~100 nm to ~1000 nm in diameter. The assembly of rod/wire-like building blocks into 3D hollow structures with a large radius of curvature is typically challenging owing to the reduced accessible contact areas between the building blocks and core template[38]. Rod/wire-like building blocks of SiO_2, iron

oxyhydroxide akaganeite (β-FeOOH), zinc oxide (ZnO), and silver cyanide (AgCN) with different aspect ratios ranging from ~1:2 to ~1:70 were also assembled into hollow supraparticles akin to complex structures achieved using other means (**Fig. 4d–g**)[39]. The robustness of our technique suggests that the C/G groups generate a strong interfacial attractive force with the template surface and that metal-phenolic complexation affords strong interactions among the assembled building blocks. Additionally, nickel nickeltetracyanonickelate ($Ni[Ni(CN)_4]$) nanosheets were selected to demonstrate the assembly capability of 2D building blocks (**Fig. 4h**), whereas cubic Prussian blue ($Fe_4[Fe(CN)_6]_3$) nanoparticles were selected as complex 3D building blocks (**Fig. 4i**). Biological 3D building blocks (i.e., *Micrococcus lysodeikticus*) could also be assembled into core–satellite and hollow supraparticles using our strategy (**Fig. 4j,k**). The assembly of cells on microparticles is useful for portable cell culture technology, cell therapy, and tissue reconstruction[40]. The hollow biological supraparticles exhibit similar structures of cellular clusters in tissues and therefore could be potentially used for the engineering of biomimetic or tissue-like hybrid materials[41].

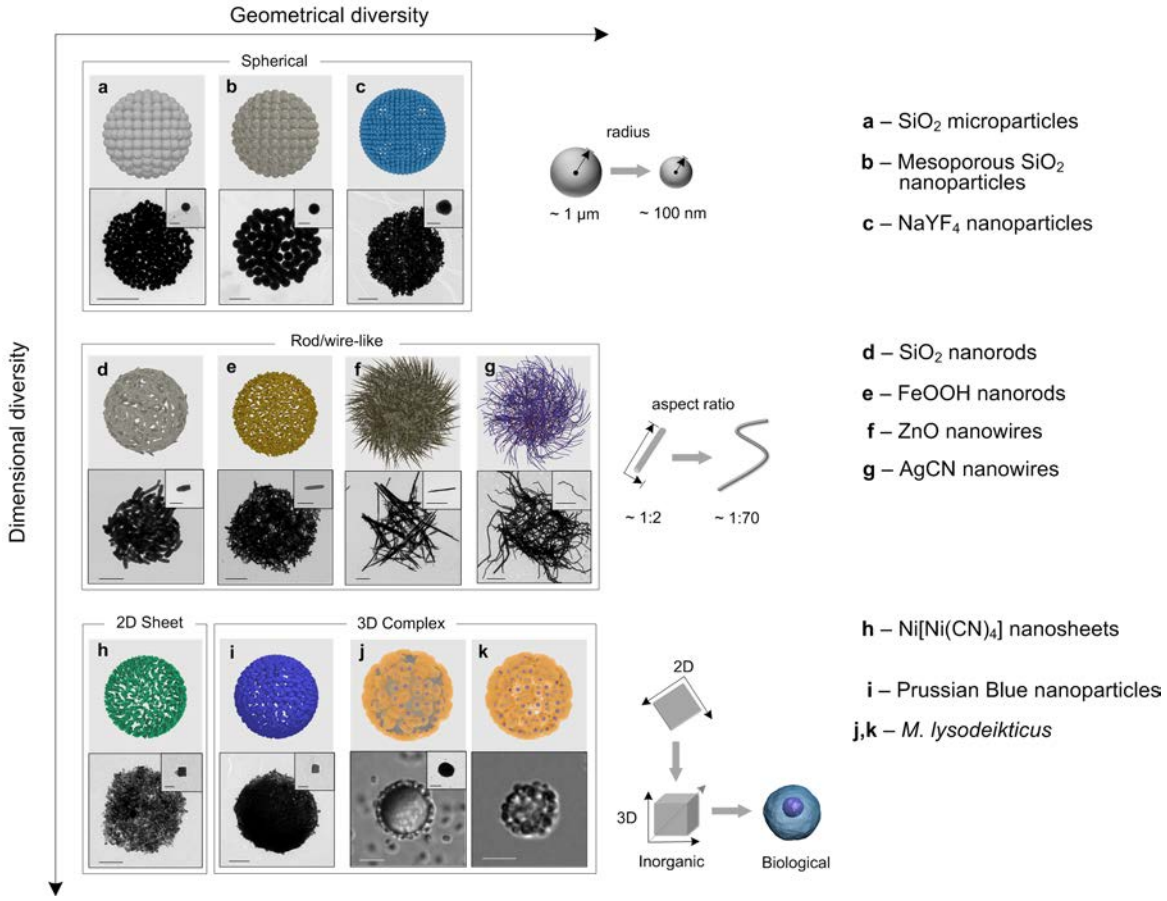

Figure 4. Analogous superstructures prepared from versatile building blocks at different dimensional scales. Computer-generated models, and associated (**a–i**) TEM and (**j,k**) differential interference contrast (DIC) microscopy images of versatile superstructures displaying different size, geometry, and composition. Images in the top rows depict basic spherical building blocks, with radii of ~100 nm, ~500 nm, and ~1 µm. Images in middle rows depict the assembly of rod/wire-like building blocks with different aspect ratios. Images in bottom rows depict the assembly of 2D and 3D cubic or complex building blocks. Scale bars are 1 µm except in **a**, **j**, and **k**, wherein the scale bars are 5 µm, and the inset images, wherein the scale bars are 1 µm (**a**), 500 nm (**b**), 100 nm (**c**), 500 nm (**d**), 200 nm (**e**), 2 µm (**f**,**g**), 100 nm (**h**,**i**), and 500 nm (**j**). **a–i** and **k** depict hollow supraparticles, whereas and **j** depicts core–satellites.

Tailoring the structure and function of supraparticle assemblies

In nature, fine-tuning of material properties can be achieved by biomolecular coordination of different metal ions[11]. This inspired us to examine whether metal ions other than Fe^{3+} could be used as cross-linking stabilizers for the formation of 3D hollow supraparticles, as different metals have specific properties, including binding constants, luminescence and coordination

sites. This provides opportunities to engineer supraparticles with diverse chemical and physical properties[30,42]. Metal ions had to be present for supraparticle formation, and five types of metal ions with different types of electron orbital structures and valencies were examined, including Fe^{3+}, Zn^{2+} (3d block), Al^{3+} (3p block), Zr^{4+} (4d block), and Ce^{3+} (4f block). High-angle annular dark-field (HAADF) TEM and corresponding energy-dispersive X-ray spectroscopy (EDS) mapping images revealed that all studied metal ions could be used for forming hollow ${}^{0.3}SiO_2$ supraparticles (**Fig. 5a**). Despite the stability of the Fe^{3+}-linked supraparticles (with respect to solvents and mechanical stirring), the latter could rapidly break down into discrete building blocks upon sonication. When the metal ion bricks were changed from Fe^{3+} to Al^{3+}, the resulting supraparticles were sensitive to pH changes. The Al^{3+}-linked hollow supraparticles disassemble in acidic environments owing to breakage of the metal-particle bonds (**Supplementary Fig. S10**).

The modular assembly method was extended to the co-assembly of different functional particles into heterogeneous supraparticles. As shown in **Fig. 5b,c**, MF particles of three different colours were co-assembled into single hollow supraparticles. The fluorescence spectra of the resulting supraparticles featured three distinct emission peaks at 426, 534, and 692 nm (**Fig. 5c**). Additionally, hierarchical hollow supraparticles with multiple components were engineered to function as drug delivery vehicles that could release an encapsulated drug and self-monitor this drug release through luminescence intensity changes (**Fig. 5d** and **Supplementary Fig. S11**). Monitoring of the drug release was achieved through energy coupling between the $NaYF_4$:Yb/Er upconversion nanoparticles and doxorubicin-loaded mesoporous SiO_2 nanoparticles. As shown in **Fig. 5e**, owing to overlap of the absorption peak of doxorubicin with the emission peak of $NaYF_4$:Yb/Er nanoparticles, the emission of $NaYF_4$:Yb/Er nanoparticles could be quenched by the loaded doxorubicin through Förster resonance energy transfer[43]. After 24 h of incubation under acidic conditions, doxorubicin

was released and the emission intensity of the supraparticles increased. These results indicate that the superstructures assembled from our modular method can exhibit efficient coupling effects between the functional building blocks, suggesting that a near-infinite number of functional hybrids could be potentially prepared using this method[1].

Although complex hierarchical superstructures can be prepared by previously mentioned methods such as LbL or block polymer self-assembly, sophisticated designs and processes are usually required for each individual component and for the assembled supraparticle as a whole[44]. In contrast, our modular assembly method allows the construction of hierarchical superstructures using facile and efficient processes (**Fig. 5f,g** and **Supplementary Fig. S12**). For example, nanoparticles (280 nm, green) were used to form first-generation supraparticles around core particles (930 nm, blue). Then, the subunit $^{0.9}$MF@$^{0.2}$PS supraparticles were co-assembled onto larger secondary core particles (15 μm, red) to form second-generation hierarchical core–satellite ^{15}PS@($^{0.9}$MF@$^{0.2}$PS) supraparticles.

One significant feature of the C/G groups is their multiple anchoring interactions on most types of interfaces[32]. Therefore, interactions between C/G-functionalized building blocks and different core template surfaces could be used to form superstructures around materials other than PS and MF. Magnetic PS/SiO_2 particles were super-assembled on the surface of human microvascular endothelial cells (HMECs) to form complex 3D bio/inorganic core–satellites (**Fig. 5h**). The HMEC-based supraparticles could be manipulated with a magnetic field (**Fig. 5i**); such a phenomenon is potentially useful for 3D cell patterning and medical diagnostics[41].

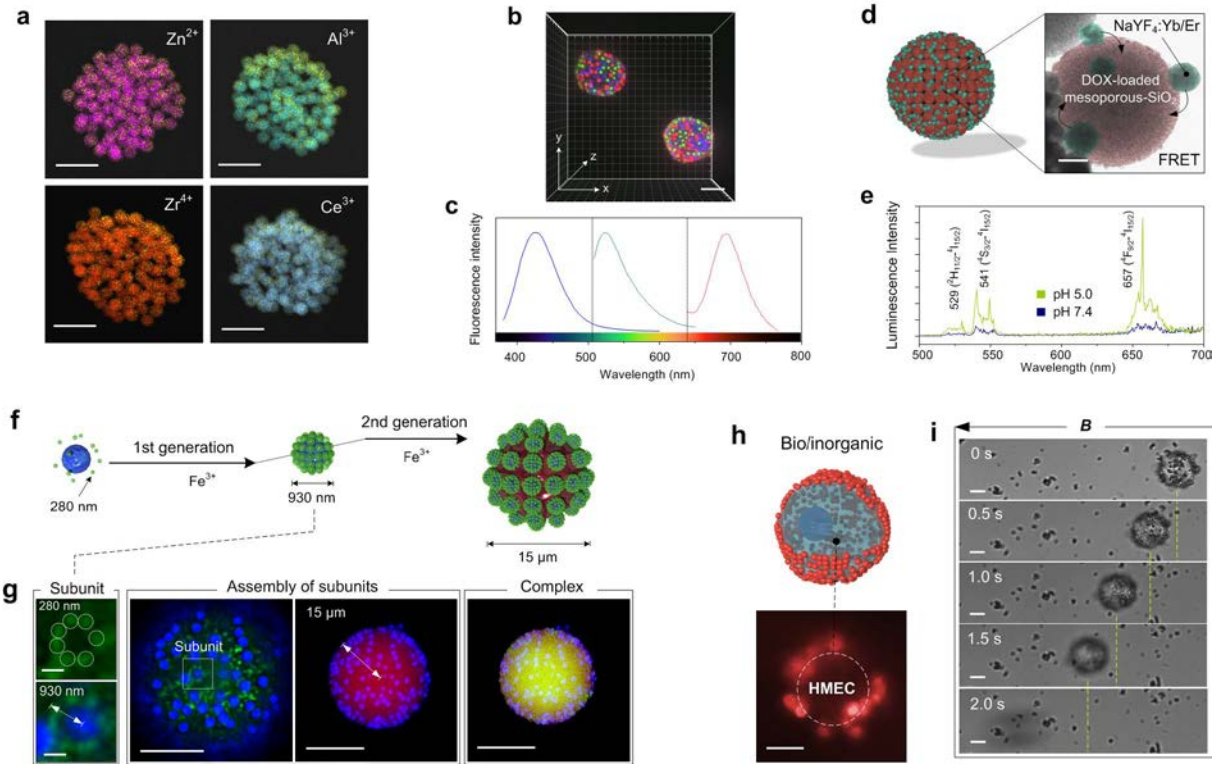

Figure 5. Structural tailorability of modular-assembled superstructures. a, Overlap images of X-ray spectroscopy (EDS) and high-angle annular dark-field (HAADF) images of hollow $^{0.3}SiO_2$ supraparticles with different metal linkages (scale bars are 1 μm). **b**, Fluorescence image of co-assembled multicomponent hollow supraparticles from different coloured fluorescent $^{0.9}$MF (melamine resin) particles (scale bar is 5 μm). **c**, Fluorescence spectra of co-assembled hollow $^{0.9}$MF supraparticle suspension excited at 360, 488, and 630 nm. **d**, Schematic representation and TEM image of hollow doxorubicin-$^{0.6}SiO_2$@$^{0.1}NaYF_4$:Yb/Er supraparticles. $NaYF_4$:Yb/Er and doxorubicin-loaded SiO_2 nanoparticles are coloured cyan and red, respectively (scale bar is 100 nm). **e**, Luminescence spectra of hollow doxorubicin-$^{0.6}SiO_2$@$^{0.1}NaYF_4$:Yb/Er supraparticles suspension in different pHs after 24 h of incubation. **f**,**g** Schematic representation and structured illumination microscopy (SIM) images of subunit $^{0.9}$MF@$^{0.2}$PS (scale bars are 200 nm) and subsequent assembly on 15-μm PS particles to obtain hierarchical ^{15}PS@($^{0.9}$MF@$^{0.2}$PS) (scale bars are 5 μm). **h**, Schematic representation and fluorescence image of core–satellite human microvascular endothelial cells (HMECs)@$^{0.9}PS/Fe_2O_3$ supraparticles. **i**, Snapshots of DIC images of HMEC@$^{0.4}SiO_2/Fe_2O_3$ taken in the presence of a magnetic field (scale bars are 5 μm).

Because of the simple modular linkage between the building blocks, the magnetic particles could be arranged with an external magnetic field and locked into a one-dimensional (1D) worm-like superstructure (**Supplementary Fig. S13**). This fast and easy magnetic-assisted assembly process could be promising for engineering tissue scaffolds, optical sensors,

and microrobots[2]. Finally, we showed that our modular method could be even extended to manufacturing at the macroscopic scale. Bio/inorganic collagen matrix (CM)@silver nanoparticles were prepared through the assembly of C/G-functionalized silver nanoparticles on 3D CM (**Supplementary Fig. S14**). These hybrid materials can be used as stretchable high-performance electromagnetic devices[45].

Conclusions

We demonstrated a highly versatile and effective methodology to prepare a large variety of superstructures assembled from a wide range of building blocks. Our method displays significant versatility in terms of size, shape, nano- and microstructure, and composition of building blocks, thus affording a number of superstructures. The modularity and simplicity of this method arise from the polyphenol-based particle surface functionalization, which enables transformation of different materials into modular bricks for superstructuring. The metal ions used for assembly can be selected from different blocks in the periodic table, resulting in superstructures with enhanced chemical diversity and structural flexibility. Colloidal-probe AFM studies revealed that the attractive force between the C/G-functionalized particles and the template substrate is the main driving force for assembly, whereas the dynamic repulsion–attraction balance between two FePN-coated surfaces results in robust particle locking after contact. MD simulations suggested that the interaction of aromatic rings between the C/G groups and a PS-based substrate played a dominant role in generating attractive interactions. We anticipate that this method will open an avenue to new simple manufacturing pathways of complex micro-/macroscale hybrid materials and devices.

References

1. Nie, Z., Petukhova, A. & Kumacheva, E. Properties and emerging applications of self-assembled structures made from inorganic nanoparticles. *Nature Nanotech.* **5**, 15–25 (2010).

2. Xu, L. *et al.* Nanoparticle assemblies: dimensional transformation of nanomaterials and scalability. *Chem. Soc. Rev.* **42**, 3114–3126 (2013).
3. Antonietti, M. & Göltner, C. Superstructures of functional colloids: chemistry on the nanometer scale. *Angew. Chem. Int. Ed.* **36**, 910–928 (1997).
4. Howes, P. D., Rana, S. & Stevens, M. M. Plasmonic nanomaterials for biodiagnostics. *Chem. Soc. Rev.* **43**, 3835–3853 (2014).
5. Chou, L. Y., Zagorovsky, K. & Chan, W. C. DNA assembly of nanoparticle superstructures for controlled biological delivery and elimination. *Nature Nanotech.* **9**, 148–155 (2014).
6. Hayward, R., Saville, D. & Aksay, I. Electrophoretic assembly of colloidal crystals with optically tunable micropatterns. *Nature* **404**, 56–59 (2000).
7. Cecchini, M. P., Turek, V. A., Paget, J., Kornyshev, A. A. & Edel, J. B. Self-assembled nanoparticle arrays for multiphase trace analyte detection. *Nature Mater.* **12**, 165–171 (2013).
8. Magasinski, A. *et al.* High-performance lithium-ion anodes using a hierarchical bottom-up approach. *Nature Mater.* **9**, 353–358 (2010).
9. Yang, S. J., Antonietti, M. & Fechler, N. Self-assembly of metal phenolic mesocrystals and morphosynthetic transformation toward hierarchically porous carbons. *J. Am. Chem. Soc.* **137**, 8269–8273 (2015).
10. Guo, S. & Sun, S. FePt nanoparticles assembled on graphene as enhanced catalyst for oxygen reduction reaction. *J. Am. Chem. Soc.* **134**, 2492–2495 (2012).
11. Degtyar, E., Harrington, M. J., Politi, Y. & Fratzl, P. The mechanical role of metal ions in biogenic protein-based materials. *Angew. Chem. Int. Ed.* **53**, 12026–12044 (2014).
12. Whitesides, G. M. & Grzybowski, B. Self-assembly at all scales. *Science* **295**, 2418–2421 (2002).
13. Schreiber, R. *et al.* Hierarchical assembly of metal nanoparticles, quantum dots and organic dyes using DNA origami scaffolds. *Nature Nanotech.* **9**, 74–78 (2014).
14. Grzelczak, M., Vermant, J., Furst, E. M. & Liz-Marzán, L. M. Directed self-assembly of nanoparticles. *ACS Nano* **4**, 3591–3605 (2010).
15. Zhang, Y., Lu, F., Yager, K. G., van der Lelie, D. & Gang, O. A general strategy for the DNA-mediated self-assembly of functional nanoparticles into heterogeneous systems. *Nature Nanotech.* **8**, 865–872 (2013).
16. Wang, L., Xu, L., Kuang, H., Xu, C. & Kotov, N. A. Dynamic nanoparticle assemblies. *Acc. Chem. Res.* **45**, 1916–1926 (2012).
17. Dinsmore, A. *et al.* Colloidosomes: selectively permeable capsules composed of colloidal particles. *Science* **298**, 1006–1009 (2002).
18. Caruso, F., Caruso, R. A. & Möhwald, H. Nanoengineering of inorganic and hybrid hollow spheres by colloidal templating. *Science* **282**, 1111–1114 (1998).
19. Xia, Y. *et al.* Self-assembly of self-limiting monodisperse supraparticles from polydisperse nanoparticles. *Nature Nanotech.* **6**, 580–587 (2011).

20. He, J., Liu, Y., Babu, T., Wei, Z. & Nie, Z. Self-assembly of inorganic nanoparticle vesicles and tubules driven by tethered linear block copolymers. *J. Am. Chem. Soc.* **134**, 11342–11345 (2012).
21. Zhao, H. *et al.* Reversible trapping and reaction acceleration within dynamically self-assembling nanoflasks. *Nature Nanotech.* **11**, 82–88 (2016).
22. Sperling, M., Velev, O. D. & Gradzielski, M. Controlling the shape of evaporating droplets by ionic strength: formation of highly anisometric silica supraparticles. *Angew. Chem. Int. Ed.* **53**, 586–590 (2014).
23. Mirkin, C. A., Letsinger, R. L., Mucic, R. C. & Storhoff, J. J. A DNA-based method for rationally assembling nanoparticles into macroscopic materials. *Nature* **382**, 607–609 (1996).
24. Alivisatos, A. P. *et al.* Organization of'nanocrystal molecules' using DNA. *Nature* **382**, 609–611 (1996).
25. Jones, M. R., Seeman, N. C. & Mirkin, C. A. Programmable materials and the nature of the DNA bond. *Science* **347**, 1260901 (2015).
26. Tan, S. J., Campolongo, M. J., Luo, D. & Cheng, W. Building plasmonic nanostructures with DNA. *Nature Nanotech.* **6**, 268–276 (2011).
27. Shenton, W., Davis, S. A. & Mann, S. Directed self-assembly of nanoparticles into macroscopic materials using antibody–antigen recognition. *Adv. Mater.* **11**, 449–452 (1999).
28. Ejima, H. *et al.* One-step assembly of coordination complexes for versatile film and particle engineering. *Science* **341**, 154–157 (2013).
29. Lee, H., Dellatore, S. M., Miller, W. M. & Messersmith, P. B. Mussel-inspired surface chemistry for multifunctional coatings. *Science* **318**, 426–430 (2007).
30. Guo, J. *et al.* Engineering multifunctional capsules through the assembly of metal–phenolic networks. *Angew. Chem. Int. Ed.* **53**, 5546–5551 (2014).
31. Tan, L. H., Xing, H. & Lu, Y. DNA as a powerful tool for morphology control, spatial positioning, and dynamic assembly of nanoparticles. *Acc. Chem. Res.* **47**, 1881–1890 (2014).
32. Wei, Q. & Haag, R. Universal polymer coatings and their representative biomedical applications. *Mater. Horiz.* **2**, 567–577 (2015).
33. Nguyen, T. D., Schultz, B. A., Kotov, N. A. & Glotzer, S. C. Generic, phenomenological, on-the-fly renormalized repulsion model for self-limited organization of terminal supraparticle assemblies. *Proc. Natl Acad. Sci. U.S.A.* **112**, E3161–E3168 (2015).
34. Hugel, T. & Seitz, M. The study of molecular interactions by AFM force spectroscopy. *Macromol. Rapid Commun.* **22**, 989–1016 (2001).
35. Rose, S. *et al.* Nanoparticle solutions as adhesives for gels and biological tissues. *Nature* **505**, 382–385 (2014).
36. Penna, M., Mijajlovic, M., Tamerler, C. & Biggs, M. J. Molecular-level understanding of the adsorption mechanism of a graphite-binding peptide at the water/graphite interface. *Soft Matter* **11**, 5192–5203 (2015).

37. Meddahi-Pellé, A. *et al.* Organ repair, hemostasis, and in vivo bonding of medical devices by aqueous solutions of nanoparticles. *Angew. Chem. Int. Ed.* **53**, 6369–6373 (2014).
38. Dang, X. *et al.* Virus-templated self-assembled single-walled carbon nanotubes for highly efficient electron collection in photovoltaic devices. *Nature Nanotech.* **6**, 377–384 (2011).
39. Bahng, J. H. *et al.* Anomalous dispersions of 'hedgehog' particles. *Nature* **517**, 596–599 (2015).
40. Jakab, K. *et al.* Tissue engineering by self-assembly and bio-printing of living cells. *Biofabrication* **2**, 022001 (2010).
41. Souza, G. R. *et al.* Three-dimensional tissue culture based on magnetic cell levitation. *Nature Nanotech.* **5**, 291–296 (2010).
42. Grindy, S. C. *et al.* Control of hierarchical polymer mechanics with bioinspired metal-coordination dynamics. *Nature Mater.* **14**, 1210–1216 (2015).
43. Dai, Y. *et al.* Up-conversion cell imaging and pH-induced thermally controlled drug release from $NaYF_4$: Yb^{3+}/Er^{3+}@hydrogel core–shell hybrid microspheres. *ACS Nano* **6**, 3327–3338 (2012).
44. Gröschel, A. H. *et al.* Guided hierarchical co-assembly of soft patchy nanoparticles. *Nature* **503**, 247–251 (2013).
45. Guo, J., Wang, X., Liao, X., Zhanga, W. & Shi, B. Skin collagen fiber-biotemplated synthesis of size-tunable silver nanoparticle-embedded hierarchical intertextures with lightweight and highly efficient microwave absorption properties. *J. Phys. Chem. C* **116**, 8188–8195 (2012).

Acknowledgements

This research was conducted and funded by the Australian Research Council (ARC) Centre of Excellence in Convergent Bio-Nano Science and Technology (project number CE140100036). This work was also supported by the ARC under the Australian Laureate Fellowship (F.C., FL120100030) and Discovery Project (F.C., DP130101846) schemes. J.G. is grateful for a scholarship under the Chinese government award for outstanding self-financed students abroad by the China Scholarship Council (CSC). This work was performed in part at the Materials Characterisation and Fabrication Platform (MCFP) at the University of Melbourne and the Victorian Node of the Australian National Fabrication Facility (ANFF). We acknowledge Fan Tian, Qiong Dai, Danzi Song, Xi Chen, Mattias Björnmalm, Matthew Faria, Quinn Besford, and Ejima Hirotaka for assistance with experiments. We thank Xiaoling Wang, Xuepin Liao, and Bi Shi for providing the skin collagen matrix and polyphenol

extracts. We also thank Matthew Penna and Patrick Charchar for useful discussions. A.J.C. and I.Y. acknowledge the generous allocation of high-performance computational resources from the Australian National Computational Infrastructure (NCI), the Western Australian computational facility (iVEC), the Victorian Partnership for Advanced Computing (VPAC), and the Victorian Life Sciences Computational Initiative (VLSCI).

Author contributions

J.G. and F.C. conceived the ideas. B.L.T. and R.R.D. conducted the AFM experiments. A.J.C. and I.Y. conceived the modelling approach and performed the MD simulations and the corresponding data analysis. Y.D. performed the luminescence measurements. J.J.R., W.Z., M.H., Y.J., and J.C. assisted with the cell experiments and contributed to the general methodology. J.G., B.L.T., A.J.C., I.Y., J.J.R., J.C., and F.C. drafted the manuscript. All authors discussed the results and commented on the manuscript.

Additional information

Supplementary information is available in the online version of the paper. Reprints and permission information is available online at http://www.nature.com/reprints. Correspondence and requests for materials should be addressed to F.C.

Competing financial interests

The authors declare no competing financial interests.

Figure captions

Figure 1. Modularization, assembly, and inter-particle locking of building blocks analogous to LEGO bricks. a, Schematic of versatile materials with different shapes, structures, compositions, and functionalities. **b**,**c**, LEGO brick-inspired modularization of building blocks through polyphenol-based particle functionalization. **d**,**e**, Modular assembly of core–satellite and hollow supraparticles with a selection of versatile modularized building blocks, templates, and metal ions. **f**,**g**, Assembly of building blocks on core particles using interfacial molecular interactions between polyphenol moieties and the substrate. **h**, Schematic and molecular structure of LEGO brick-inspired linkage between polyphenol-functionalized particles.

Figure 2. Modular assembly of SiO_2, fluorescent melamine resin (MF) particles, and polystyrene (PS) particles into spherical 3D superstructures. a, Differential interference contrast (DIC) images of core–satellite $^{10}PS@^{1}SiO_2$ supraparticles (scale bars are 10 μm and 2 μm in the inset image). **b–d**, Sliced, 3D structured illumination microscopy (SIM) images, and reconstructed model of core–satellite $^{10}PS@^{0.5}MF$ supraparticles (scale bars are 5 μm). **e**,**f**, SEM images of hollow $^{0.3}SiO_2$ supraparticles prepared through critical point drying (CPD) technique (scale bars are 2 μm in **e** and 500 nm in **f**). **g**,**h**, TEM images of hollow $^{0.3}SiO_2$ supraparticles prepared as ultra-thin sliced (**g**) and air-dried (**h**) specimens (scale bars are 2 μm).

Figure 3. Colloidal-probe AFM studies of modular assembly. a–c, Schematic of disperse building block particles and large core templates (**a**), assembly of building block particles on the surface of core templates (**b**), and inter-particle locking of assembled building block particles on core templates (**c**). **d**,**e** Schematic and representative force–distance curves of FePN-coated SiO_2-attached probes approaching bare PS particles with neutral (**d**) and negative (**e**) surface charges. **f**, Schematic and representative force–distance curves of FePN-coated SiO_2-attached probe approaching an FePN-coated planar glass substrate.

Figure 4. Analogous superstructures prepared from versatile building blocks at different dimensional scales. Computer-generated models, and associated (**a–i**) TEM and (**j**,**k**) differential

interference contrast (DIC) microscopy images of versatile superstructures displaying different size, geometry, and composition. Images in the top rows depict basic spherical building blocks, with radii of ~100 nm, ~500 nm, and ~1 μm. Images in middle rows depict the assembly of rod/wire-like building blocks with different aspect ratios. Images in bottom rows depict the assembly of 2D and 3D cubic or complex building blocks. Scale bars are 1 μm except in **a**, **j**, and **k**, wherein the scale bars are 5 μm, and the inset images, wherein the scale bars are 1 μm (**a**), 500 nm (**b**), 100 nm (**c**), 500 nm (**d**), 200 nm (**e**), 2 μm (**f**,**g**), 100 nm (**h**,**i**), and 500 nm (**j**). **a–i** and **k** depict hollow supraparticles, whereas and **j** depicts core–satellites.

Figure 5. Structural tailorability of modular-assembled superstructures. a, Overlap images of X-ray spectroscopy (EDS) and high-angle annular dark-field (HAADF) images of hollow $^{0.3}SiO_2$ supraparticles with different metal linkages (scale bars are 1 μm). **b**, Fluorescence image of co-assembled multicomponent hollow supraparticles from different coloured fluorescent $^{0.9}$MF (melamine resin) particles (scale bar is 5 μm). **c**, Fluorescence spectra of co-assembled hollow $^{0.9}$MF supraparticle suspension excited at 360, 488, and 630 nm. **d**, Schematic representation and TEM image of hollow doxorubicin-$^{0.6}SiO_2$@$^{0.1}NaYF_4$:Yb/Er supraparticles. $NaYF_4$:Yb/Er and doxorubicin-loaded SiO_2 nanoparticles are coloured cyan and red, respectively (scale bar is 100 nm). **e**, Luminescence spectra of hollow doxorubicin-$^{0.6}SiO_2$@$^{0.1}NaYF_4$:Yb/Er supraparticles suspension in different pHs after 24 h of incubation. **f**,**g** Schematic representation and structured illumination microscopy (SIM) images of subunit $^{0.9}$MF@$^{0.2}$PS (scale bars are 200 nm) and subsequent assembly on 15-μm PS particles to obtain hierarchical ^{15}PS@($^{0.9}$MF@$^{0.2}$PS) (scale bars are 5 μm). **h**, Schematic representation and fluorescence image of core–satellite human microvascular endothelial cells (HMECs)@$^{0.9}$PS/Fe_2O_3 supraparticles. **i**, Snapshots of DIC images of HMEC@$^{0.4}SiO_2/Fe_2O_3$ taken in the presence of a magnetic field (scale bars are 5 μm).

Methods

See Supplementary Materials for a detailed description of materials, building block particles, diverse superstructure assembly, characterizations, colloidal-probe AFM measurements, and molecular dynamics simulation methods.

Metal coordination-based particle functionalization. The building block particles were suspended in Milli-Q (MQ) water or DPBS buffer solution (0.5–5% w/v). TA and $FeCl_3$ solutions were added to the building block particle suspension to achieve the final concentrations of TA (0.24 mM) and Fe^{3+} (0.24 mM). Then, MOPS buffer solution (pH 8.0, 100 mM) was added to raise the solution pH. An Fe-TA (iron-phenolic) network (FePN) was formed and used for functionalizing the surface of the building block particles with catechol/galloyl (C/G) groups[28,30]. The functionalized building block particles were washed 3–4 times with MQ water to remove the excess Fe-TA complexes. In the washing process, the particles were spun down by centrifugation and the supernatant was removed. The centrifugation speeds used for the different particles were varied and optimized to avoid particle aggregation: ~50 nm – 8000 *g*, 10 min; 100–200 nm – 800 *g*, 15 min; ~500 nm – 1000 *g*, 5 min; ~800 nm – 1000 *g*, 2 min; and ~1 μm – 1000 *g*, 1.5 min. Particle monodispersity was necessary for the particle assembly process.

Oxidation reaction-based particle functionalization. It has been demonstrated that functionalization of building blocks can be achieved via a mussel-inspired polydopamine (PDA) coating[29]. This functionalization process was used for the formation of core–satellite and hollow supraparticles, thus highlighting the versatility of surface chemistry in the modular assembly method. Briefly, dopamine (12 mg) was dissolved in MQ water (4.4 mL). The suspension of building blocks was mixed with the dopamine solution to achieve the final dopamine concentration of 2 mg/mL. Polymerization of dopamine was allowed to proceed for 2–3 h in Tris buffer solution (pH 8.5, 10 mM) with constant shaking in ambient air at room temperature (~25 °C) at 1 atmosphere pressure. The PDA-functionalized building block particles were obtained after washing 3–4 times with MQ water to remove the excess PDA. The resulting particles' monodispersity was necessary for the subsequent particle assembly process on larger core particles. Therefore, centrifugation speeds were optimized to avoid aggregation.

Supraparticle assembly. The superstructural assembly of building block particles can occur after mixing with larger core particles (or templates, e.g., PS, MF particles (0.1–5% w/v), cells, collagen matrix). During the assembly process, the mixing suspension was vortexed for 10–60 s to instigate collisions between the building blocks and cores (templates). Sonication may be applied to assist the dispersion of particles. After particle mixing, inter-particle locking was achieved by adding metal ions (final concentration: 0.24 mM $FeCl_3$, $AlCl_3$, $ZrCl_4$, $CeCl_3$, or $ZnSO_4$) and an equal volume of MOPS buffer solution (pH 8.0, 100 mM). The C/G groups from two different particles can complex with the same metal ions (clusters) to form the inter-particle bridging. Core–satellite supraparticles were obtained after washing 3–5 times with MQ water to remove the free building blocks and template particles. The centrifugation speeds used for the different core–satellite supraparticles were varied and optimized to avoid particle aggregation: 100–200 nm – 800 *g*, 15 min; ~1 μm – 1000 *g*, 1.5 min, and ~3.5 μm – 1000 *g*, 1 min.

Formation of hollow supraparticles. Metal-phenolic coordination bonds between particles provide robust linkages for the construction of hollow superstructures. In the core (template) removal process, the core–satellite supraparticles were spun down by centrifugation and washed 3–4 times with THF. The arrangement of the building particles could be stabilized accordingly to maintain a hollow superstructural architecture. During the THF washing process, the hollow supraparticles were spun down by centrifugation and the supernatant was removed. The centrifugation speeds used for the different hollow supraparticles were varied and optimized to avoid particle aggregation: 100–200 nm – 800 *g*, 15 min; ~1 μm – 1000 *g*, 1.5 min, and ~3.5 μm – 1000 *g*, 1 min. After removal of the core, the hollow supraparticles were transferred to the desired solvents (MQ water or buffer solutions). Note that metal ions were required for SP formation.

Hierarchical supraparticle assembly. The C/G-functionalized building blocks do not easily form free linkages with each other owing to electrostatic repulsion forces between them. Therefore, the interactions between the C/G groups and core particles play a dominant role in the dynamic force interactions, leading to subsequent assembly of supraparticles with larger cores. Green fluorescence polystyrene particles (280 nm) were functionalized with C/G groups using the protocol in Supplementary Section S5. The functionalized particles were then mixed with 930 nm blue fluorescence MF particles and vortexed for 10–30 s (sonication may be applied to assist the dispersion of particles). $FeCl_3$ solution and an equal volume of

MOPS buffer solution (pH 8.0, 100 mM) were added to effect inter-particle locking (final concentration of Fe^{3+}: 0.24 mM). $^{0.9}$MF@$^{0.2}$PS core–satellite supraparticles were obtained by washing three times with MQ water. $^{0.9}$MF@$^{0.2}$PS core–satellite supraparticles were directly mixed with 15-μm red fluorescence PS particles and vortexed for 10–30 s. $FeCl_3$ solution and an equal volume of MOPS buffer solution (pH 8.0, 100 mM) were added to induce secondary inter-particle locking (final concentration of Fe^{3+}: 0.24 mM). Hierarchical ^{15}PS@($^{0.9}$MF@$^{0.2}$PS) core–satellite supraparticles were obtained by washing three times with MQ water.

Author/s:
Guo, J;Tardy, BL;Christofferson, AJ;Dai, Y;Richardson, JJ;Zhu, W;Hu, M;Ju, Y;Cui, J;Dagastine, RR;Yarovsky, I;Caruso, F

Title:
Modular assembly of superstructures from polyphenol-functionalized building blocks

Date:
2016-12-01

Citation:
Guo, J., Tardy, B. L., Christofferson, A. J., Dai, Y., Richardson, J. J., Zhu, W., Hu, M., Ju, Y., Cui, J., Dagastine, R. R., Yarovsky, I. & Caruso, F. (2016). Modular assembly of superstructures from polyphenol-functionalized building blocks. NATURE NANOTECHNOLOGY, 11 (12), pp.1105-1111. https://doi.org/10.1038/NNANO.2016.172.